

Micromagnetically integrated numerical model of spin pumping based on spin diffusionMarkus Gattringer^{1,*}, Claas Abert¹, Florian Bruckner¹, Andrii Chumak², and Dieter Suess¹¹*Physics of Functional Materials, University of Vienna, Kolingasse 14–16, Vienna, Austria*²*Nanomagnetism and Magnonics, University of Vienna, Boltzmanngasse 5, Vienna, Austria*

(Received 16 May 2022; revised 30 June 2022; accepted 30 June 2022; published 18 July 2022)

We present a nanoscopic numerical model of spin pumping, complete with spin-torque effects, as an extension of a spin-diffusion solver. The model is fully integrated in a micromagnetics finite-element framework. It is shown that this model can recreate analytical solutions for standard problems. Furthermore, the Gilbert damping of a propagating magnon can be properly modeled. The model can be used to examine spin-pumping effects, and those caused by it, e.g., inverse spin Hall, on a nanoscopic scale.

DOI: [10.1103/PhysRevB.106.024417](https://doi.org/10.1103/PhysRevB.106.024417)**I. INTRODUCTION**

The interaction between localized and mobile spins in magnetic materials has long been understood. It has been modeled in various forms [1–3] and is successfully used to model and design spintronic devices [4,5]. In those cases, the interest lies in the effect that a spin current (usually originating from a charge current) has on the dynamics (i.e., precession) of local magnetization. But the reverse is also true (by virtue of Onsager’s reciprocity relation [6]): The precession of magnetization has an effect on spin current, in that it can be the origin of it. This is generally known as spin pumping. More specifically, the term means the outflow of spins from a magnetic material into a nonmagnetic material [7]. This effect has been proven in numerous experiments (e.g., Refs. [7–9]).

As such, it enables one to create a spin current without a corresponding charge current. The effect is too weak to realistically compete with direct spin-injection and spin-Hall methods for spin-transfer torque and spin-orbit torque applications (see Ref. [6] for some formulaic comparisons)—while spin torque and spin pumping are reciprocal, the amount of spin current (and therefore spin torque) generated by spin transfer can easily be many magnitudes larger than by spin pumping. It is, however, used, in conjunction with the inverse-spin-Hall effect, as a detection scheme for magnons, i.e., spin waves [8,10,11]. Moreover, the spin accumulation created by the effect changes the local magnetization dynamics by generally increasing Gilbert damping and decreasing the rate of precession [2,7].

Analytical treatments of spin pumping are generally calculated using the formalism of Büttiker *et al.* [12]. As this does not lend itself too well to numerical computations, a numerical model in a micromagnetic setup is still missing. Note that Omelchenko *et al.* used such a Büttiker-type formulation for their numerical results [13], with their system using single spins.

Such a micromagnetic implementation is of prime interest, since this can use all the already implemented magnetization dynamics, and would therefore be well suited to support magnonic simulations (and experiments). Based upon the spin-diffusion model [3], we now introduce such a model. Aside from our own previous work on spin diffusion [14], and associated research (e.g., Ref. [15]), the spin-diffusion model is also employed by other groups (cf. Refs. [16,17]). But even though a formulation of the spin-diffusion model incorporating spin pumping has been presented already in 2004 [2], to date, numerical implementations of the model have not incorporated spin pumping. Note that the package exhibited in Ref. [17] is able to simulate spin pumping, but only by a prebuilt current term (similarly to Ref. [13]).

First, we show the derivation of spin pumping in the spin-diffusion framework and the resulting changes to the governing equation. We then modify our self-consistent spin-diffusion model [14], which is part of our finite-element (FE)-based solver suite MAGNUM.PI, an evolution of the earlier MAGNUM.FE [18], to incorporate those changes. We then test the model against two literature cases where analytical terms in a spin-diffusion setup have been presented, for diffusionless pumping in bulk, and pumping from the surface of a magnetic insulator. Finally, to demonstrate the implementation in a dynamical, micromagnetic case, we explore the damping of a magnon by spin pumping.

II. DERIVATION AND METHOD

Magnetism is a property emerging from the spin property of a quantum-mechanical object. In a first-order approximation, the spins in a material can be decomposed into those supplied by quasistatic objects, i.e., cations localized on their lattice sites, and those from mobile objects, i.e., conduction electrons. We can then treat the spins, or, in a continuous sense, the magnetization of those conduction electrons, as a transport quantity. This makes it possible to start with a Boltzmann-type transport equation for the magnetization

*markus.gattringer@univie.ac.at

carried by conduction electrons \mathbf{M}_e [2],

$$\frac{\partial \mathbf{M}_e}{\partial t} = -\nabla \cdot \widehat{\mathbf{j}}_s - \frac{J}{\hbar} \mathbf{M}_e \times \mathbf{m} - \frac{1}{\tau_{sf}} \mathbf{s}, \quad (1)$$

where $\widehat{\mathbf{j}}_s$ is the magnetization (or spin) current matrix. \mathbf{m} is then the normalized magnetization of the material (i.e., the metal cations without the conduction electrons) and \mathbf{s} is the spin accumulation. τ_{sf} is the spin-flip time of the conduction electrons, J the exchange coupling between the conduction electrons and the metal cations, and \hbar is the reduced Planck's constant. To link the magnetization of the conduction electrons and the spin accumulation together, the former can be decomposed into a component parallel to \mathbf{m} and an additional one, such that

$$\mathbf{M}_e = \chi_e M_S \mathbf{m} + \mathbf{s}. \quad (2)$$

These two components represent a permanently existing one (where it is assumed that the conduction electrons' spins will align in the cations field at equilibrium), and the spin accumulation as an additional one (the deviation from that equilibrium). This does not mean that the two components are necessarily orthogonal to each other; for multi-magnetic-layer systems (as in Ref. [13]) they are not. For the systems described herein, with single magnetic layers, they are. Therefore $\mathbf{m} \cdot \mathbf{s} = 0$, which can be shown for the analytical results in the next section. M_S is the saturation magnetization of the material. We use the prefactor that was introduced by

Takahashi [19]. It offers the advantage that it can be easily calculated using material parameters that are already in use in our framework. He defines the susceptibility of the conduction electrons χ_e as

$$\chi_e = \mu_0 \mu_B^2 n(\mathcal{E}_F) \frac{J}{\hbar \mu_0 \gamma_e M_S} = \frac{\mu_B C_0 J}{e^2 M_S D_0}, \quad (3)$$

where $C_0 = n(\mathcal{E}_F) e^2 D_0 / 2$ is used, a variant of Sommerfeld's conductivity formula. This susceptibility is a product of the paramagnetic susceptibility of the conduction electrons and a dimensionless interaction constant. μ_0 is the magnetic constant, μ_B Bohr's magneton, γ_e the free-electron gyromagnetic ratio (i.e., $2\mu_B/\hbar$), e the elementary charge, $n(\mathcal{E}_F)$ the density of states for conduction electrons at the Fermi level, D_0 the electronic diffusion constant, and $C_0 = \sigma/2$ the conductivity half.

Inserting Eq. (2) in (1), we can apply the adiabatic approximation $\partial \mathbf{s} / \partial t = \mathbf{0}$ (due to the relaxation timescale of \mathbf{s} being much smaller than of \mathbf{m}) and yield [2]

$$\chi_e M_S \frac{\partial \mathbf{m}}{\partial t} = -\nabla \cdot \widehat{\mathbf{j}}_s - \frac{J}{\hbar} \mathbf{s} \times \mathbf{m} - \frac{1}{\tau_{sf}} \mathbf{s}. \quad (4)$$

This is the standard form of spin pumping and is generally used for analytical treatments. If the left-hand side of Eq. (4) is not zero, i.e., magnetization is precessing, a spin current will be generated, or pumped. For numerical applications, one needs to understand that the left-hand side of Eq. (4) (i.e., the driving term for spin pumping) is a function of \mathbf{s} itself, since

$$\begin{aligned} \frac{\partial \mathbf{m}}{\partial t} &= -\frac{\mu_0 \gamma_e}{1 + \alpha^2} \left\{ \mathbf{m} \times \left(\mathbf{H}_{\text{eff}} + \frac{J}{\hbar \mu_0 \gamma_e M_S} \mathbf{s} \right) + \alpha \mathbf{m} \times \left[\mathbf{m} \times \left(\mathbf{H}_{\text{eff}} + \frac{J}{\hbar \mu_0 \gamma_e M_S} \mathbf{s} \right) \right] \right\} \\ &= \mathbf{T}(\mathbf{H}_{\text{eff}}) - \frac{J}{\hbar M_S (1 + \alpha^2)} [\mathbf{m} \times \mathbf{s} + \alpha \mathbf{m} \times (\mathbf{m} \times \mathbf{s})]. \end{aligned} \quad (5)$$

This is the well-known explicit form of the Landau-Lifshitz-Gilbert (LLG) equation [20], where the spin torque generated by spin pumping has been split off from the remaining fields ($\mathbf{H}_{\text{eff}} = \mathbf{H}_{\text{Zee}} + \mathbf{H}_{\text{ex}} + \mathbf{H}_{\text{demag}} + \mathbf{H}_{\text{ani}} + \dots$), that are then combined in the torque operator $\mathbf{T}(\mathbf{H}_{\text{eff}})$. α is the Gilbert damping parameter. The spin accumulation generated by spin pumping exerts an influence on the causative precession. In analytical treatises this will resolve itself in the end, but for explicit numerical calculations, this influence will need to be considered directly in Eq. (4). Therefore, we insert Eq. (5) and combine the spin-accumulation terms, leading to

$$\begin{aligned} \chi_e M_S \mathbf{T}(\mathbf{H}_{\text{eff}}) &= -\nabla \cdot \widehat{\mathbf{j}}_s - \frac{J}{\hbar} \left(1 + \frac{\chi_e}{1 + \alpha^2} \right) \mathbf{s} \times \mathbf{m} \\ &\quad - \left(\frac{1}{\tau_{sf}} + \frac{\chi_e J \alpha}{\hbar (1 + \alpha^2)} \right) \mathbf{s} \\ &\quad + \frac{\chi_e J \alpha}{\hbar (1 + \alpha^2)} (\mathbf{m} \cdot \mathbf{s}) \mathbf{m}. \end{aligned} \quad (6)$$

This form now enables self-consistent numerical computation of the spin accumulation as it incorporates the effects of spin torque on the precessional motion of magnetization. To solve Eq. (6), we need to calculate the $\mathbf{T}(\mathbf{H}_{\text{eff}})$ operator. In our setup,

this is achieved by a hybrid FE/boundary element method (incorporating Ref. [21]). Equation (6) is then solved on the same FE mesh, with the magnetization current of the form of

$$\widehat{\mathbf{j}}_s = -2 D_0 \nabla \otimes \mathbf{s}, \quad (7)$$

and the homogeneous Neumann boundary condition of

$$(\mathbf{n} \cdot \nabla) \mathbf{s} = \mathbf{0}, \quad (8)$$

where \mathbf{n} is the boundary normal. This condition also applies to the analytical treatments in the next section.

The solution method for the resulting system of differential equations is given in Ref. [22]. Using the computed \mathbf{s} and $\mathbf{T}(\mathbf{H}_{\text{eff}})$ operator, we can then integrate Eq. (5) by an implicit backward differentiation scheme, as given in Ref. [23].

As the spin accumulation (or spin current) resulting from spin pumping is not directly measured experimentally, but usually via the inverse-spin-Hall effect, the inclusion of it will be outlined. In such a case, Eq. (7) modifies to

$$\widehat{\mathbf{j}}_s = 2 \beta C_0 \frac{\mu_B}{e} \mathbf{m} \otimes \nabla u - 2 D_0 \nabla \otimes \mathbf{s} + \frac{\mu_B}{e} \Theta_{\text{SH}} \widehat{\mathbf{e}} \mathbf{j}_e. \quad (9)$$

This now includes a drift term resulting from potential differences [3], as well as a term describing the spin-Hall effect

according to Dyakonov [24]. β is the electronic (magnetization) polarization, u the charge potential, Θ_{SH} the spin-Hall angle, and $\hat{\epsilon}$ the Levi-Civita symbol.

In addition, a second Boltzmann-type equation is set up, describing the charge current [3], also including a term for the spin-Hall interaction. Instead of solving Eq. (6), now the system of both Boltzmann-type equations has to be solved for \mathbf{s} and u to also yield the effects of the spin-orbit interaction. This process is detailed in Ref. [25].

It is important to note that the spin-diffusion equation can only be applied in a conductive material, or else no spin current can exist. For spin pumping, this is exacerbated by the fact that the driving term is always zero as there are no conduction electrons. Application of this model to spin pumping from nonconductive material needs a special treatment in the simulation; this will be shown in the following section.

III. COMPUTATION AND RESULTS

To validate our model with analytical solutions from the literature (that are rewritten to use our constants), we extract values from the numerical computation from a defined state. Spin accumulation is extracted directly as a computation result, while the modification of the dynamical behavior is determined by projecting the total torque vector onto the cross-product basis of the LLG and suitable renormalization. We compare those values against those obtained from analytical formulas in the same state. Note that the provided analytical terms for the spin accumulation are achieved by solving Eq. (6) and thus do not concur with those found by the other authors [as they solve Eq. (4)]. This originates from the fact that we explicitly compute the spin accumulation. The core point here is that the analytical treatments that are referenced and our numerical computations take a different path to their goal, but should agree in the end result, namely the enhanced Gilbert damping and decreased rate of precession.

A. Bulk system

We first consider the bulk system calculated by Zhang and Li [2]. The authors suppose that the system is diffusionless, i.e., $\nabla \otimes \mathbf{m} \propto \hat{\mathbf{j}}_s = \emptyset$ (where \otimes denotes the outer product; the result is then a matrix), which is true for single-material bulk systems with homogeneous magnetization. Under that constraint, we can solve Eq. (6) to yield

$$\mathbf{s} = -\frac{\Gamma_{\text{BS}} \chi_e M_S}{1 + \Gamma_{\text{BS}}^2} \frac{\hbar(1 + \alpha^2)}{J(1 + \alpha^2 + \chi_e)} \times [\mathbf{T}(\mathbf{H}_{\text{eff}}) + \Gamma_{\text{BS}} \mathbf{m} \times \mathbf{T}(\mathbf{H}_{\text{eff}})]. \quad (10)$$

Here, we define

$$\Gamma_{\text{BS}} = \frac{\tau_{\text{sf}} J(1 + \alpha^2 + \chi_e)}{\hbar(1 + \alpha^2) + \tau_{\text{sf}} \alpha \chi_e J}. \quad (11)$$

Solving Eq. (4) under the same constraint, and inserting the solution into Eq. (5), one can recreate the form of the original LLG by introducing modified γ_e and α parameters,

$$\gamma_{\text{SP}} = \gamma_e \frac{1 + \Gamma_{\text{B}}^2}{1 + \Gamma_{\text{B}}^2(1 + \chi_e)} \quad (12)$$

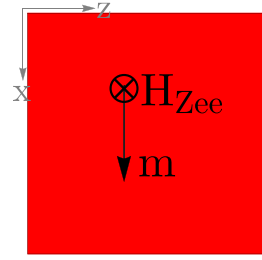


FIG. 1. Bulk system, $10 \times 10 \times 10$ nm.

and

$$\alpha_{\text{SP}} = \frac{\alpha(1 + \Gamma_{\text{B}}^2) + \Gamma_{\text{B}} \chi_e}{1 + \Gamma_{\text{B}}^2(1 + \chi_e)}, \quad (13)$$

where $\Gamma_{\text{B}} = \tau_{\text{sf}} J / \hbar$. This is a rewritten form of the result of Ref. [2]. These modifications to the Gilbert damping and to the rate of precession lead, as had been mentioned in the Introduction, to an increase of the former and to a decrease of the latter. The damping from spin pumping is an important mechanism of damping in magnetic materials, especially for multilayer systems (as will be seen in the next section).

To test our implementation against this result, we set up a cube as shown in Fig. 1 with homogeneous magnetization. Such a setup, and having no internal interactions (i.e., $\mathbf{H}_{\text{eff}} = \mathbf{H}_{\text{Zee}}$), makes the system diffusionless—it behaves as if it only consists of a single spin. The system parameters were chosen to simulate permalloy and are listed in Table I. The only exception is the exchange coupling strength J , or, via the relation $\lambda_c = \sqrt{2 D_0 \hbar} / J$, the coupling length λ_c . Variations in the coupling length, although not achievable in experiments, provide a representative way to test the implementation. For the analytical calculation of Eq. (10) we set, as per Fig. 1,

$$\mathbf{T}(\mathbf{H}_{\text{eff}}) = -\frac{\mu_0 \gamma_e \|\mathbf{H}_{\text{Zee}}\|}{1 + \alpha^2} [(0, 0, 1)^T - \alpha(0, 1, 0)^T]. \quad (14)$$

Figure 2 shows the y and z components of the average computed spin accumulation compared to the values from Eq. (10). It can be seen that the results are in good agreement with each other. The x component (not depicted) should equal zero, but numerical computation yields a finite value in the aAm^{-1} range due to numerical errors.

Figure 3 shows the modified gyromagnetic ratio γ_{SP} and damping parameter α_{SP} , compared to the values from Eqs. (12) and (13). Once again, the results are in good agreement with each other. The damping generated by spin pumping is about half the intrinsic damping at maximum. For realistic values of the coupling length for such a system,

TABLE I. Bulk system.

Quantity	Value
M_S	900 kAm^{-1}
C_0	1 MSm^{-1}
D_0	$10 \text{ cm}^2 \text{ s}^{-1}$
λ_{sf}	4 nm
$\ \mathbf{H}_{\text{Zee}}\ $	7.96 kAm^{-1}

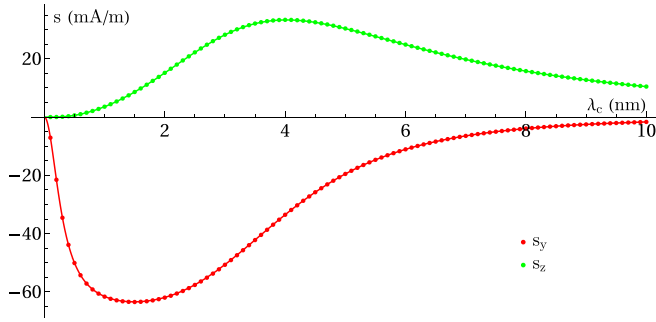


FIG. 2. y and z components of \mathbf{s} , as functions of λ_c for the bulk system. Data points are computed values, and the solid line the analytical prediction; $\alpha = 0$.

$\lambda_c \approx 3$ nm, it is still $\approx 40\%$. The damping from spin pumping therefore constitutes an important part of the total damping in bulk systems.

B. Layer system

The second system we consider is the interface system calculated by Takahashi (see pp. 1462–1465 in Ref. [19]). His analytical formulation has been specifically introduced to extend the spin diffusion's applicability to nonconductive material. Such a system, consisting of a nonconductive magnetic material and a nonmagnetic conductor, is a good representation of the yttrium iron garnet (YIG, $Y_3Fe_5O_{12}$)/platinum systems often employed in magnonics. This section is called a *layer* because we model the interaction as an actual layer in the numerical computation. The localized interaction effectively decouples the $\mathbf{s}\text{-}\mathbf{m}$ term in Eq. (6) and enables solution of the diffusion equation in the case of homogeneous magnetization, using Eq. (7), as a homogeneous equation with the boundary term as

$$\mathbf{s}(x) = -\frac{\Gamma_{IS} \chi_e M_S}{1 + \Gamma_{IS}^2} \frac{\hbar(1 + \alpha^2)}{J(1 + \alpha^2 + \chi_e)} \cosh\left(\frac{L-x}{\lambda_{sf}}\right) \times \text{sech}\left(\frac{L}{\lambda_{sf}}\right) [\mathbf{T}(\mathbf{H}_{eff}) + \Gamma_{IS} \mathbf{m} \times \mathbf{T}(\mathbf{H}_{eff})]. \quad (15)$$

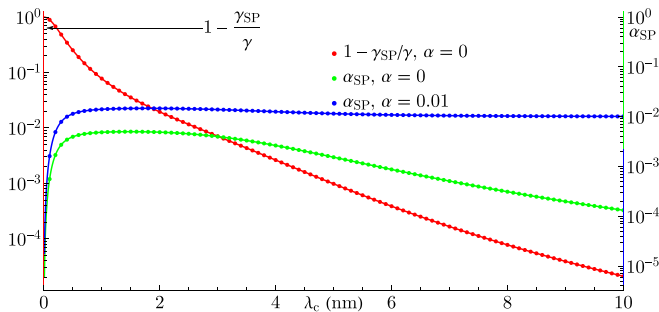


FIG. 3. γ_{SP} (left axis) and α_{SP} (right axis), as logarithmic functions of λ_c for the bulk system. To facilitate logarithmic plotting for γ_{SP} , values have been recalculated. Data points are computed values, and solid lines the analytical prediction.

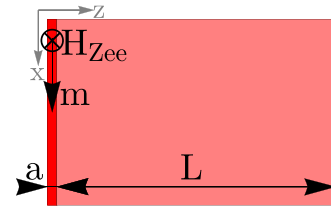


FIG. 4. Layer system with a 10×10 nm cross section in the xy -plane. The red part with thickness $a = 0.5$ nm is magnetic and conducting, and the pink one only conducting.

Here, L is the length of the conductor and $\lambda_{sf} = \sqrt{2D_0 \tau_{sf}}$ is the spin-flip length. We define

$$\Gamma_{IS} = \frac{a}{\lambda_{sf}} \coth\left(\frac{L+a}{\lambda_{sf}}\right) \Gamma_B, \quad (16)$$

where a is the effective pumping length. This is to account for the fact that the $\mathbf{s}\text{-}\mathbf{m}$ coupling is not an interface effect and has to be given some coupling length. The saturation magnetization is, after all, a volume average, and needs to be transformed into an effective surface magnetization to be used as a boundary term. In the same way, the spin-torque term in the LLG also gains a modulation length. Since it can be naively expected (and is confirmed by the computations, at least within numerical reason) that this effective torque length d is equal to a , the contributions cancel out and Eqs. (12) and (13) remain unchanged, except for

$$\Gamma_B \rightarrow \frac{a}{\lambda_{sf}} \coth\left(\frac{L+a}{\lambda_{sf}}\right) \Gamma_B, \quad (17)$$

the same modulation as above. The additional hyperbolic cotangent, modulating Γ (or a), results from the finite-sized system and the fact that the dropoff of spin accumulation is slower than for an open system. Hence more spin accumulation exists in the interaction layer, and it behaves similar to an increased interaction length.

To test against this result, we set up a bar as shown in Fig. 4, with homogeneous magnetization in the magnetic region with thickness 0.5 nm. As the tetrahedral resolution is also 0.5 nm, this results in a single layer of tetrahedra carrying magnetization; hence we expect $a = d = 0.5$ nm. The utilization of a distinctive interaction layer originates from the necessities of FE. As a differential equation is solved not on points in space (as with finite differences), but by volume integration over tetrahedra (see Ref. [26] for details of the method), interactions on surfaces (other than full boundary conditions) are not possible. Even more, since material parameters are defined as discontinuous functions (to model material interfaces), Eq. (3)

TABLE II. Layer system.

Quantity	Magnetic	Conducting
M_S	140 kAm $^{-1}$	None
C_0		4.5 MSm $^{-1}$
D_0		50 cm 2 s $^{-1}$
λ_{sf}		14 nm
$\ \mathbf{H}_{Zee}\ $	7.96 kAm $^{-1}$	None

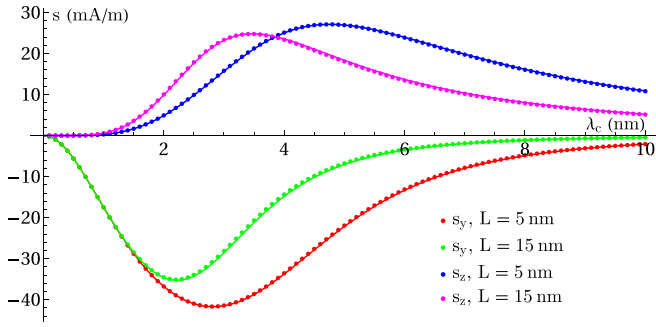


FIG. 5. y and z components of \mathbf{s} , as functions of λ_c for the layer system, both long and short spin sinks. Data points are computed values, and the solid lines the analytical prediction; $\alpha = 0$.

is not even defined at the interface. And since the physical interaction is not really a surface interaction anyway, we prefer the layer method to implement any approximate surface terms.

Again all internal interactions are ignored. The system parameters are chosen to simulate a YIG/Pt system and are listed in Table II. It is important to understand here that the red part is simulated to be both magnetic and fully conducting—it is an interaction layer that is both YIG and Pt, at least simulationwise. $\mathbf{T}(\mathbf{H}_{\text{eff}})$ is identical to the preceding section.

Figure 5 shows the y and z components of the average computed spin accumulation in the magnetic region, compared to the values from Eq. (15). Results again agree, but not as good as for the bulk system. This is to be expected: Whereas the bulk system eliminates all nonlocalities by eliminating diffusion, here the computation has to be done on a mesh, introducing discretization errors.

Figure 6 shows the average modified gyromagnetic ratio γ_{SP} and damping parameter α_{SP} in the magnetic region, compared to the values from Eqs. (12) and (13). Once again, the results are in good agreement with each other. The additional damping generated by the spin torque is very noticeable: We use $\alpha = 2 \times 10^{-4}$, which is now increased by two orders of magnitude in the interaction layer. The difference in L now also leads to different damping curves.

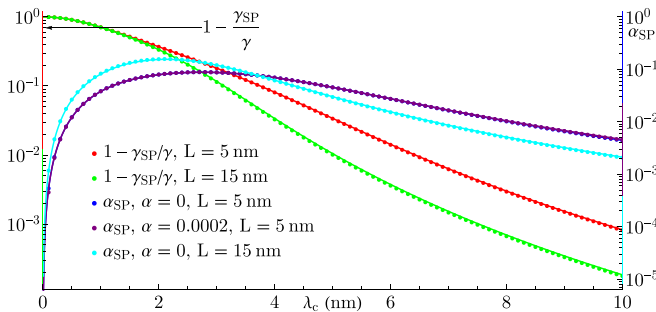


FIG. 6. γ_{SP} (left axis) and α_{SP} (right axis), as logarithmic functions of λ_c for the layer system, both long and short spin sinks. To facilitate logarithmic plotting for γ_{SP} , values have been recalculated. Data points are computed values, and solid lines the analytical prediction.

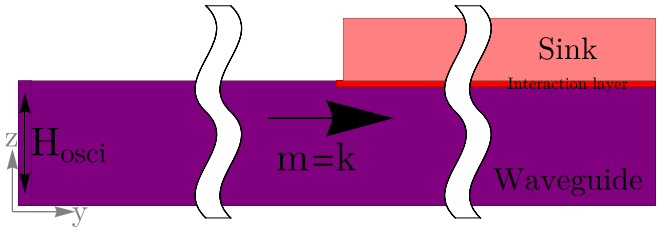


FIG. 7. The magnonic damping system. The magnetic waveguide with $10 \times 1251 \times 10$ nm is in purple, the magnetic and conducting interaction layer with thickness 0.5 nm is in red, and the conducting spin sink with thickness 5 nm is in pink.

The dependence of the achieved damping upon the spin sink length is also evident from Fig. 6. This has also been shown in prior experiments [13].

C. Magnonic damping

To test our implementation against a dynamic (and somewhat real-world) case, we look into the propagation of a magnon, the disturbance of the local magnetization by a localized linearly polarized external field. The increased Gilbert damping due to the spin torque from spin pumping should quickly suppress the magnon.

To this end we extend the layer system to the fully fledged waveguide seen in Fig. 7. The length of the waveguide is 1251 nm, of which the first 1 nm is subject to a linearly polarized external field \mathbf{H}_{osci} , oscillating in the z direction and driving the magnon (with both the initial magnetization and the wave vector \mathbf{k} of the magnon in the y direction). After 251 nm, a spin sink layer is placed atop the waveguide, with a corresponding interaction layer beneath it. The material parameters are shown in Table III, with A being the exchange strength and K the anisotropy strength. Note that $\alpha = 0$, hence all damping observed originates from spin pumping.

The setup of a nonconducting magnetic material was chosen to limit the computation of spin pumping to a smaller part of the system. Furthermore, the material parameters were modified to achieve a small wavelength exchange magnon and high damping. In addition, demagnetization-field contributions were not computed, both for performance and implementation reasons. Instead, we simulate the restoring force on the magnetization by applying an uniaxial anisotropy field along the y axis. The system parameters are specifically

TABLE III. Magnonic damping system.

Quantity	Waveguide	Interaction	Sink
M_S	140 kAm $^{-1}$		None
A	200 fJm $^{-1}$		None
C_0	None	10 MSm $^{-1}$	
D_0	None	50 cm 2 s $^{-1}$	
λ_{sf}	None	2 nm	
λ_c	None	2 nm	None
K	10 kJ/m 3		None
$\ \mathbf{H}_{\text{osci}}\ $	First 1 nm: 79.6 kAm $^{-1}$		None
f	First 1 nm: 30 GHz		None

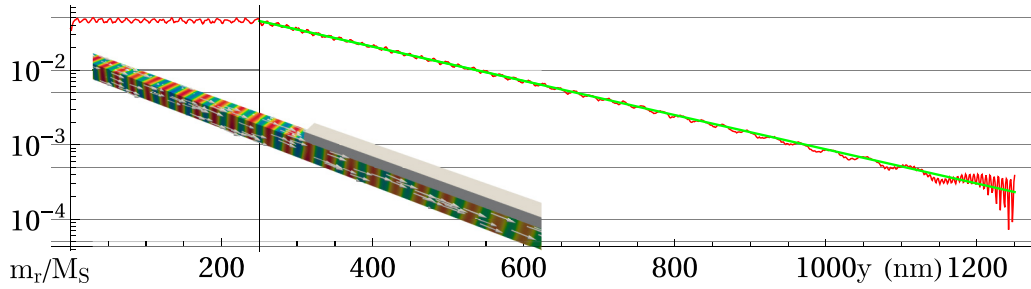


FIG. 8. Transversal component of \mathbf{m} (=wave amplitude) at $x = z = 5$ nm (the waveguide center), as a logarithmic function of the coordinate for the magnonic damping system after 2.4 ns. Red are computed values, and green is a fitted exponential decay with the magnon free path $l = 190$ nm. The black vertical line marks the beginning of the spin sink layer. The inset shows a three-dimensional (3D) snapshot of the simulation configuration, with color coded values of m_z .

chosen to demonstrate the implementation's capabilities and not to mimic an actual experimental setup.

Figure 8 shows the transversal component of the magnetization along the waveguide centerline after 2.4 ns. The magnon has penetrated the whole waveguide, with the spin-torque-enhanced damping successfully suppressing the magnon along its path. Fitting a simple exponential function to the magnetization for $y > 250$ nm (where the waveguide is covered by the spin sink), a free path of $l = 190$ nm can be obtained. It is clearly visible that considerable damping exists, even with $\alpha = 0$.

Figure 9 shows the modified gyromagnetic ratio γ_{SP} and damping parameter α_{SP} along a line at $z = 9.5$ nm, compared to the values from Eqs. (12) and (13). Although the propagating magnon exhibits nonhomogeneous, wavelike precession (in space), the modified parameters do not reflect that behavior and behave as if the precession is indeed homogeneous. Also, the deviation from "normal" values ($\gamma_{SP} = \gamma$ and $\alpha_{SP} = 0$) is less pronounced than expected. Both effects can be attributed to the cross diffusion of spin accumulation in the interaction layer: The analytical solution for homogeneous magnetization assumes the effect of only the locally produced spin accumulation on the precessional motion. For a magnon, spin accumulation produced at some point can diffuse to other points in the vicinity, effecting the precession there as well. In return, the effect on the precession at the point where it was produced is reduced. This cross diffusion would then equilibrate the spin accumulation, generally reducing it, and therefore its effects. This behavior would generally depend upon the relation between the magnon wavelength and λ_{sf} .

The rapid oscillations at the end of the waveguide ($y > 1100$ nm) most likely originate from numerical errors. The

magnetization is almost coaligned with the longitudinal axis, which is a regime where the integration errors from numerically solving Eq. (5) are easily of the same magnitude as the precession angle. There is some additional structure for γ_{SP} , including noticeable steps (around 700 and 900 nm). The nature of those is currently not known.

IV. CONCLUSION

We have presented a nanoscopic numerical spin-pumping solver, based upon an earlier spin-diffusion solver, fully integrated into a micromagnetics scheme. It was shown that our implementation can replicate the solutions obtained by analytical means for some standard systems, without introducing additional material parameters. Furthermore, we have shown that we can now properly model the propagation characteristics of a magnon under the influence of spin-pumping effects, i.e., decreased precession and increased damping.

We expect that the implementation can be employed in magnonic simulations. As such, we are currently using it in our own research, where we compute spin-Hall voltages out from magnon-generated spin pumping. A corresponding publication is forthcoming.

ACKNOWLEDGMENT

Work for this publication has been completed within the framework of the FWF Project No. I 4917-N "Non-reciprocal 3D architectures for magnonic functionalities."

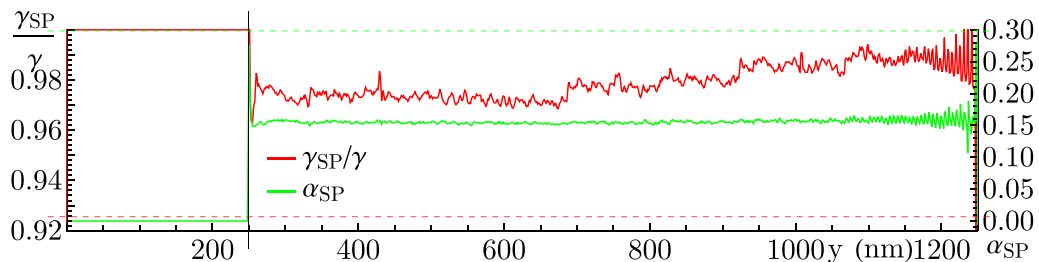


FIG. 9. γ_{SP} (left axis) and α_{SP} (right axis) at $x = 5$ nm, $z = 9.5$ nm (the interface of the waveguide and the interaction layer), as functions of the coordinate for the magnonic damping system after 2.4 ns. The black vertical line marks the beginning of the spin sink layer; the dashed lines mark the corresponding expected analytical values from Eqs. (12) and (13).

- [1] J. C. Slonczewski, *J. Magn. Magn. Mater.* **247**, 324 (2002).
- [2] S. Zhang and Z. Li, *Phys. Rev. Lett.* **93**, 127204 (2004).
- [3] S. Zhang, P. M. Levy, and A. Fert, *Phys. Rev. Lett.* **88**, 236601 (2002).
- [4] G. E. Rowlands and I. N. Krivorotov, *Phys. Rev. B* **86**, 094425 (2012).
- [5] S. Pathak, C. Youm, and J. Hong, *Sci. Rep.* **10**, 2799 (2020).
- [6] A. Brataas, Y. Tserkovnyak, G. E. W. Bauer, and P. J. Kelly, *Spin Pumping and Spin Transfer* (Oxford University Press, Oxford, U.K., 2017).
- [7] Y. Tserkovnyak, A. Brataas, and G. E. W. Bauer, *Phys. Rev. Lett.* **88**, 117601 (2002).
- [8] Y. Kajiwara, K. Harii, S. Takahashi, J. Ohe, K. Uchida, M. Mizuguchi, H. Umezawa, H. Kawai, K. Ando, K. Takanashi, S. Maekawa, and E. Saitoh, *Nature (London)* **464**, 262 (2010).
- [9] K. Ando, S. Takahashi, J. Ieda, Y. Kajiwara, H. Nakayama, T. Yoshino, K. Harii, Y. Fujikawa, M. Matsuo, S. Maekawa, and E. Saitoh, *J. Appl. Phys.* **109**, 103913 (2011).
- [10] C. W. Sandweg, Y. Kajiwara, A. V. Chumak, A. A. Serga, V. I. Vasyuchka, M. B. Jungfleisch, E. Saitoh, and B. Hillebrands, *Phys. Rev. Lett.* **106**, 216601 (2011).
- [11] A. V. Chumak, A. A. Serga, M. B. Jungfleisch, R. Neb, D. A. Bozhko, V. S. Tiberkevich, and B. Hillebrands, *Appl. Phys. Lett.* **100**, 082405 (2012).
- [12] M. Büttiker, H. Thomas, and A. Prêtre, *Z. Phys. B* **94**, 133 (1994).
- [13] P. Omelchenko, E. Girt, and B. Heinrich, *Phys. Rev. B* **100**, 144418 (2019).
- [14] C. Abert, M. Ruggeri, F. Bruckner, C. Vogler, A. Manchon, D. Praetorius, and D. Suess, *Sci. Rep.* **6**, 16 (2016).
- [15] C. Abert, F. Bruckner, C. Vogler, and D. Suess, *AIP Adv.* **8**, 056008 (2018).
- [16] M. Sturma, C. Bellegarde, J.-C. Toussaint, and D. Gusakova, *Phys. Rev. B* **94**, 104405 (2016).
- [17] S. Lepadatu, *J. Appl. Phys.* **128**, 243902 (2020).
- [18] C. Abert, L. Exl, F. Bruckner, A. Drews, and D. Suess, *J. Magn. Magn. Mater.* **345**, 29 (2013).
- [19] S. Takahashi, in *Handbook of Spintronics* (Dordrecht, 2016), pp. 1445–1480.
- [20] T. L. Gilbert, *IEEE Trans. Magn.* **40**, 3443 (2004).
- [21] D. Fredkin and T. Koehler, *IEEE Trans. Magn.* **26**, 415 (1990).
- [22] M. Ruggeri, C. Abert, G. Hrkac, D. Suess, and D. Praetorius, *Phys. B: Condens. Matter* **486**, 88 (2016).
- [23] D. Suess, V. Tsiantos, T. Schrefl, J. Fidler, W. Scholz, H. Forster, R. Dittrich, and J. J. Miles, *J. Magn. Magn. Mater.* **248**, 298 (2002).
- [24] M. I. Dyakonov, *Phys. Rev. Lett.* **99**, 126601 (2007).
- [25] C. Abert, *Eur. Phys. J. B* **92**, 120 (2019).
- [26] C. Johnson, *Numerical Solution of Partial Differential Equations by the Finite Element Method* (Dover, New York, 2009).